ELSEVIER

Contents lists available at ScienceDirect

Spectrochimica Acta Part A: Molecular and Biomolecular Spectroscopy

journal homepage: www.journals.elsevier.com/spectrochimica-acta-part-a-molecular-and-biomolecular-spectroscopy





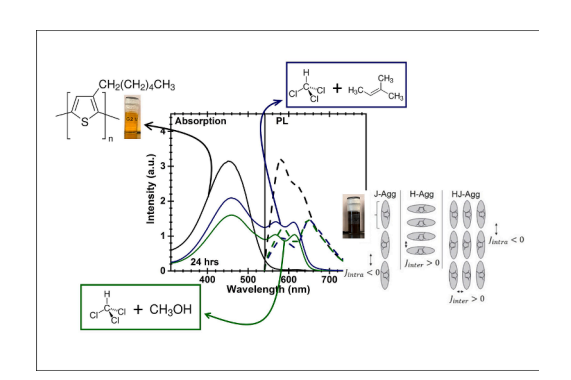
What is the significance of the chloroform stabilizer C_5H_{10} and its association with MeOH in concentration-dependent polymeric solutions?

Huan Nguyen^a, Ruan L.S. Lima^b, Newton M. Barbosa Neto^{b,*}, Paulo T. Araujo^{a,*}

HIGHLIGHTS

- Amylene (C₅H₁₀) limits the lifespan of stabilized chloroform (CHCl₃) as a good solvent.
- Metanol (MeOH) produces similar stabilization of pure CHCl₃ when compared with C₅H₁₀.
- The combination of C₅H₁₀ and MeOH leads to additional routes for controlling interchain interactions

GRAPHICAL ABSTRACT



ARTICLE INFO

Keywords:
Absorption
Photoluminescence
P3HT
Methanol
Chloroform
Aggregate formation

$A\ B\ S\ T\ R\ A\ C\ T$

The understanding of excitonic transitions associated with polymeric aggregates is fundamental, as such transitions have implications on coherence lengths, coherence numbers and inter- and intra-chain binding parameters. In this context, the investigation of efficient solvents and other ways to control polymer aggregate formation is key for their consolidation as materials for new technologies. In this manuscript, we use Poly(3-hexothiophene) (P3HT) as a probe to investigate the significance of amylene (C_5H_{10}) and its association with methanol (MeOH) in both pure and C_5H_{10} -stabilized chloroform (CHCl₃)-based polymeric solutions. Using the intensity ratio between the first and second vibronic transitions of the P3HT H-aggregates formed, values for their exciton bandwidths and interchain interactions are obtained and correlated with the presence of C_5H_{10} and MeOH as agents determining the CHCl₃ quality.

1. Introduction

The understanding and subsequent characterization of polymeric semiconducting devices has been of heightened interest as the drive for cost effective, high yield and easily processable devices pushes research interests forward [1–21]. The reproducibility and efficiency of these organic devices are intimately connected with ability of polymers to form films with high-quality aggregates and crystalline domains [1–21]. Recently, new polymers, polymeric structures, and strategies for the development of more efficient organic devices have been explored

E-mail addresses: barbosaneto@ufpa.br (N.M.B. Neto), paulo.t.araujo@ua.edu (P.T. Araujo).

^a Department of Physics and Astronomy, University of Alabama, Tuscaloosa, AL, USA

^b Institute of Natural Sciences, Federal University of Para, Belem, PA, Brazil

^{*} Corresponding authors.

[1-21]. In one hand, Bi et al. [10] achieved 31 % efficiency in organic photovoltaic cells (OPVs) under indoor light using polymer donors with enhanced crystallinities such as series PB3, PB4 and PB5 based on thiadiazole (TDZ), 4,8-bis(5-(2-ethylhexyl)thiophen-2-yl)benzo[1,2b:4,5-b']dithiophene (BDTT) and fluorinated BDT-T (BDT-T-2F). On the other hand, Smeets et al. [11] explored the synthesis of PM6 and D18 to overcome poor reproducibility organic devices' performance, while Wang et al. [15] demonstrated that POM-Cl-based all-polymer OPV cells enable rarely high JSC and fill factor (FF). Such polymers have been considered as prime candidates for numerous applications (OPVs, photodetectors, charge transport, and solubility/miscibility properties, via rational design of their constituent donor and acceptor building blocks). Benzo[1,2-b:4,5-b']difuran (BDF) based wide bandgap-conjugated polymers, PFCT-2F and PFCT-2Cl, have also been explored to overcome limitations of BDF-based structures due to aggregation properties and unfavorable active layer morphology [14]. In addition, thiazolothiazole (TzTz)-thiophene copolymers (PTzBT and PTzBTE) have been explored as alternatives for applications using π -conjugated polymers with higher crystallinity [12]. A series of all-organic dielectric polymer composites have been fabricated by blending the n-type molecular 1,4,5,8-naphthalenetetracarboxylic semiconductor (NTCDA) with polyetherimide (PEI). Such composited have led to leakage current reductions and improvements in the breakdown strength and energy storage properties at high temperatures [13]. Despite these recent developments, Poly(3-hexothiophene) (P3HT) is still a strong and well-studied player in the field [1,6,27-35].

Polymeric aggregates are traditionally understood as intra- vs interchain phenomena [6,8,27–32,36–45]. Casting P3HT as an example, Fig. 1 shows two traditional types of aggregates classified as H-aggregates (side-by-side stacking of neighboring chains) and J-aggregates (tip-to-tail stacking of neighboring chains). Fig. 1 also displays the so-called HJ-aggregate, which is an interplay between H- and J-aggregate made possible through variation of the polymers inter (J_{inter}) and intra (J_{intra}) chain coulombic coupling [6,8,27–32,36–45]. Each of these aggregates possesses unique optoelectronic properties, including well-defined photoluminescence (PL) and absorption (Abs) spectral signatures [27–32,39–41,44–46]. In fact, variations in excitonic coupling in the development of each aggregate formation results in varying spectral

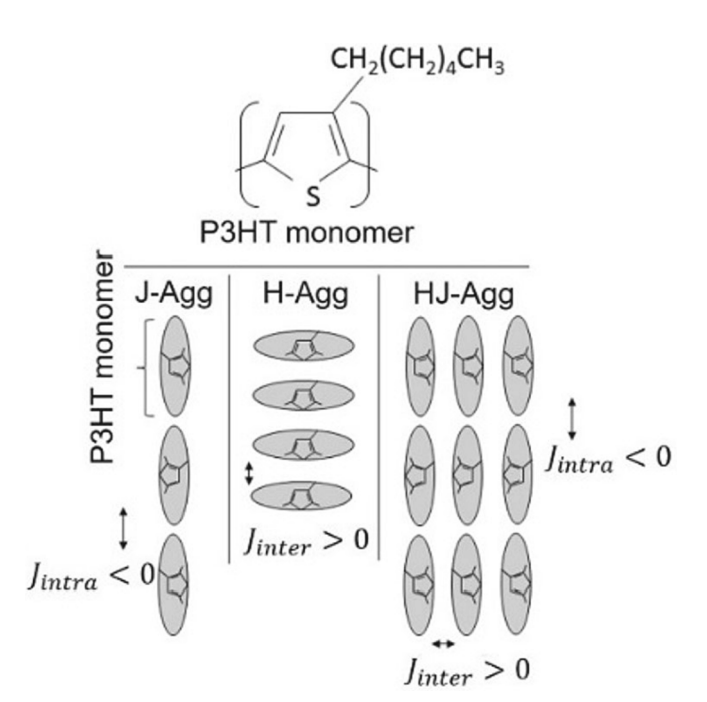


Fig. 1. (a) The P3HT repeat monomer with schematic representations of J-, H-, and HJ- aggregates. The coupling constants J_{inter} and J_{intra} are shown for clarity.

signatures. For example, the formation of J-aggregates is a result of negative excitonic coupling with $J_{intra}<0$ and $J_{inter}=0$ which subsequently allows for 0–0 emission at low temperatures. Alternatively, H-aggregate formations are a result of positive excitonic coupling with $J_{inter}>0$ and $J_{intra}=0$ which leads to a forbidden 0–0 emission at low temperatures. In HJ-aggregates ($J_{intra}\neq0$ and $J_{inter}\neq0$), for example, there is a competition between intra- and inter-chain interactions [39–41,44–46].

Theoretical developments demonstrate that J-, H-, and HJ-aggregate PL and Abs signatures are altered with variation of $J_{\rm inter}$ and $J_{\rm intra}$ [39–41,44–46]. In one hand, the ratio of the PL peak intensity of the 0–0 and 0–1 transitions $(I_{PL}^{0-0}/I_{PL}^{0-1})$ is used to determine the coherence number $(N_{\rm coh})$ and length (l_0) . On the other hand, the ratio of the Abs first (A_1) and second (A_2) vibronic progressions (A_1/A_2) and of the third (A_3) vibronic progression and A_2 (A_3/A_2) are both <1 (>1) for H- (J- and HJ-) aggregates. The H- (J- and HJ-) aggregate A_1/A_2 ratio decreases (increases) with increasing $J_{\rm inter}$ ($J_{\rm intra}$), while the opposite behavior is observed for the A_3/A_2 ratio. In addition, the H- (J- and HJ-) aggregate $I_{PL}^{0-0}/I_{PL}^{0-1}$ ratio increases (decreases) with increasing temperature. Altogether, these ratios are rather convenient to determine the different types of aggregates as well as to evaluate quality and efficiency of solvents to form and control such aggregates through the fine-tuning of both $J_{\rm inter}$ and $J_{\rm intra}$ [39–41,44–46].

Several strategies have been proposed to controllably aggregate a variety of polymers [4,6,8,10-27,30-32,47-62]. All of them exploring different solvents and parameters such as molecular weights, synthetic methods, external stimuli (e.g. pressure and temperature), and concentration [4,6,8,10-27,30-32,47-62]. Notably, P3HT has been a model polymer in such studies. Reichmanis and co-workers photoinduced aggregation of P3HT in solution using continuous UV light [60], and more recently Barbosa Neto et al. [61] demonstrated a new photoinduced approach using pulsed visible light to generate highly ordered P3HT Jand HJ-aggregate structures. In addition, Panzer and co-workers [30] utilized temperature to investigate phase transitions and the controllable formation of distinct P3HT H-aggregates in tetrahydrofuran (THF) solutions. In terms of solvents, chloroform (CHCl₃) stabilized with amylene (C₅H₁₀) has been a champion choice as it is widely considered as an excellent and versatile solvent for several polymers, including P3HT. Pure CHCl3 is usually avoided since it tends to degrade more easily than stabilized ones.

In this work, we use P3HT solutions as probes (backed-up by theory, as discussed above) to investigate in greater detail the role of stabilizers in CHCl3. Most often, studies using CHCl3 neglect the effects of stabilizers in the aggregation process. Our preliminary results, however, showed that even though stabilizers are used in very small amounts, and even though they retard CHCl3 degradation, they also render the stabilized CHCl₃ a worse solvent when compared with the pure CHCl₃. Such results led us to investigate more deeply the effect of C5H10 in the effectiveness of stabilized CHCl3 as a good solvent. We also explored methanol MeOH, as well as its combination with C₅H₁₀ as alternative CHCl₃ stabilization routes. We show the following main results: (1) C₅H₁₀ limits the lifespan of stabilized CHCl₃ as a good solvent, leading to aggregate formation in 24 h after solution preparation; (2) MeOH produces similar stabilization of pure CHCl₃ when compared with C₅H₁₀; and (3) the combination of both C₅H₁₀ and MeOH opens up additional routes for controlling the J_{inter} magnitude, as C_5H_{10} limits the MeOH action in CHCl3.

2. Experimental details

2.1. Materials

All materials and reagents were used as received. Poly(3-hexothiophene) (P3HT) (>98 % head-to-tail regioregular, average Mn $54\,000-75\,000$, $99.995\,\%$; Mn/Mw ≤ 2.5 , electronic graded from Sigma

Aldrich) was dissolved in both chloroform (CHCl $_3$) stabilized with amylene (C_5H_{10}) (Sigma-Aldrich, containing 100–200 ppm amylenes as stabilizer; ≥ 99.5 %) and pure CHCl $_3$ (Sigma-Aldrich; ≥ 99.9 %) at an initial concentration of 0.45 mg/mL. This original solution was then placed on a hot plate (Curtin Matheson 267–914) at 45 °C for 45 min. A magnetic stirrer bar was placed inside the solution vial in order to achieve a better dissolving process. The original solutions were then further diluted in order to obtain the two values of concentration used here: 0.005 mg/mL and 0.05 mg/mL. The diluted solutions were then stirred on a hot plate at 45 °C for additional 45 min to achieve isolated-chain (amorphous chains) state. The solutions were then stored in a dark box to avoid photo-degradation.

2.2. Absorption

Absorption spectra are obtained using an Agilent Cary 50 spectrophotometer running dual-beam mode. All measurements are performed in ambient conditions. Solutions are always transferred from vials to a glass cuvette upon measurements.

2.3. Photoluminescence

Photoluminescence spectra are collected through an in-house designed setup utilizing an Andor iDus 401 series model DV401A CCD with Shamrock model 303i spectroscope containing 300-line-per-milimeter grating. The CCD and spectroscope are controlled via Andor Solis computer interface software. The main laser source is an OPLS (Optically Pumped Semiconductor Diode) Sapphire 532–50 CW CDRH laser, which produces vertically polarized light at 532 nm. All measurements are performed in ambient conditions. Solutions are always transferred from vials to a glass cuvette upon measurements.

3. Results and discussion

Two distinct P3HT solutions were prepared at concentrations 0.005 mg/mL (from now on low concentration) and 0.05 mg/mL (from now on high concentration) using as solvents, pure CHCl₃ (from now on CHCl₃), CHCl₃ stabilized with C_5H_{10} (from now on CHCl₃ + C_5H_{10}), and CHCl₃ and CHCl₃ + C_5H_{10} mixed with distinct MeOH aliquots (from now on CHCl₃ + MeOH and CHCl₃ + C_5H_{10} + MeOH, respectively). All the PL and Abs measurements were performed just after solution preparation (i.e. 0 hrs) and 24 h later. In overall, the amount of C_5H_{10} in the solutions is about 10^6 less than the amount of MeOH added.

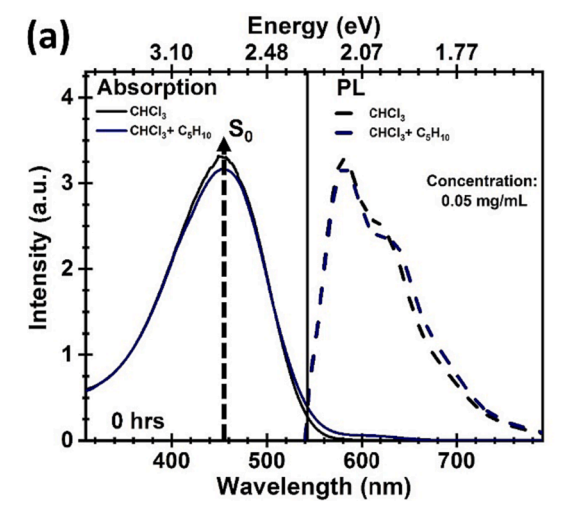
3.1. $P3HT/CHCl_3$, $P3HT/CHCl_3 + C_5H_{10}$ and $P3HT/CHCl_3 + MeOH$ solutions at low and high concentrations

Fig. 2 shows representative Abs and PL spectra from P3HT/CHCl₃ and P3HT/CHCl₃ + C₅H₁₀ solutions at concentration 0.05 mg/mL measured at 0 hrs and 24 h later. As observed in Fig. 2(a), at 0 hrs both Abs (solid curves) and PL (dashed curves) spectra from both solutions exhibit clear signatures of isolated chains (i.e. more disordered chains forming intrachain states) with no signs of aggregate formation [27-35,60-62]. However, as shown in Fig. 2(b), the same solutions measured 24 hrs later exhibit completely distinct results: the P3HT/ CHCl3 solution (black solid and dashed curves) still exhibits spectral signatures that are typical from isolated chains [27-35,60-62]; in contrast the $P3HT/CHCl_3 + C_5H_{10}$ solution (navy solid and dashed curves) shows clear evidence of aggregate formation with wellstructured vibronic progressions (first (A₁) and second (A₂) progressions, respectively). As seen in Table 1 the A₁/A₂ ratio is 0.96, and this value along with the well-structured ordered phase in the Abs spectrum suggest the establishment of weakly interacting H-aggregate states [30,31,39-41,44-46,60-62]. Due to the weakly interacting character of such H-aggregates, we understand that both the inner filter (IF) and the self-absorption (SA) phenomena are taking place in the PL spectra [63], and the overall behavior agrees well with results by Panzer and co-workers [30] that in their temperature-related studies, also

Table 1 Values for the A_1/A_2 ratio, A_3/A_2 ratio, exciton bandwidth (W) and interchain interaction (I_{inter}) for different solutions and concentrations.

P3HT/CHCl ₃ solutions: low (high) concentrations					
MeOH aliquots (μL)	A_1/A_2	A_3/A_2	W(meV)	J _{Inter} (meV)	
0	_	_	_	-	
90	0.95 (0.99)	0 (0)	13 (0.5)	3 (0.14)	
270	0.95 (0.77)	0.85 (0.92)	13 (71)	3 (18)	
450	0.89 (0.72)	0.85 (0.92)	32 (90)	8 (22)	

P3HT/CHCl ₃ + C ₅ H ₁₀ solutions: low (high) concentrations						
MeOH aliquots (μL)	$\mathbf{A}_1/\mathbf{A}_2$	A_3/A_2	W(meV)	J _{Inter} (meV)		
0	0.85 (0.96)	0 (0)	44 (10)	11 (2)		
90	0.93 (0.96)	0.82 (0.80)	21 (10)	5 (2)		
270	0.93 (0.91)	0.82 (0.80)	21 (26)	5 (7)		
450	0.99 (0.85)	0.72 (0.84)	2 (45)	0.57 (11)		



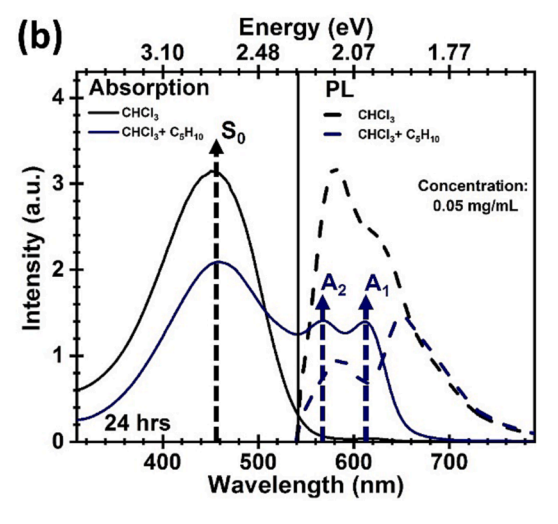


Fig. 2. Absorption (Abs) (solid curves) and Photoluminescence (PL) (dashed curves) spectra for P3HT/CHCl $_3$ (black curves) and P3HT/CHCl $_3$ + C $_5$ H $_{10}$ (navy curves) high concentration solutions at 0 hrs (a), and 24 hrs (b). The center peaks for the vibronic progressions in (b) are $A_1=613\,\mathrm{nm}$ and $A_2=568\,\mathrm{nm}$. All the figures: the center peak for the isolated chains (i.e. amorphous phase) is $S_0=455\,\mathrm{nm}$.

observed H-aggregate formation in P3HT/THF solutions. It is important to comment that no significant evidence of aggregation is observed between 0 and 24 hrs. Therefore, within this time interval, both P3HT/CHCl $_3$ and P3HT/CHCl $_3$ + C_5H_{10} are equally good for applications that require solutions with isolated chain properties. After such a time interval, it becomes noticeable that the stabilization of CHCl $_3$ comes with a cost: the P3HT/CHCl $_3$ + C_5H_{10} solutions shows clear signs of crystallization (ordered-phase) and PL self-absorption, while the P3HT/CHCl $_3$ solutions remain amorphous.

To better understand the role of C₅H₁₀ as a stabilizer and aggregation agent, MeOH was used as a stabilizer for CHCl3 and as an agent for CHCl₃ + C₅H₁₀ quality tuning. As shown in Fig. 3, the P3HT/CHCl₃ + MeOH (90 μ L) solution at 0.05 mg/mL, in which 90 μ L of MeOH is added to CHCl3, leads to similar aggregate formation when compared to P3HT/ $CHCl_3 + C_5H_{10}$ (A₁/A₂ = 0.96; Fig. 2(b)). The A₁/A₂ ratio is 0.99 (see Table 1), indicating similar weakly interacting H-aggregate formation with a larger predominance of the isolated chain properties within the aggregates [30,31,39-41,44-46,60-62]. Once again, the PL shows clear evidence of both IF and SA phenomena [63], and the overall behavior agrees well with the results observed for the P3HT/CHCl₃ + C₅H₁₀ solution. Although Fig. 3 shows PL and Abs spectra for solutions measured 24 hrs after preparation, the aggregate formation in P3HT/CHCl₃ + MeOH solutions occurs instantaneously and remains unchanged over 24 hrs. In spite of the distinct chemical composition observed for C₅H₁₀ and MeOH, no signs of PL and Abs blue- or red-shift is observed (i.e. no signs solvatochromism phase transitions or [30,31,39-41,44-46,60-62].

PL and Abs measurements of solutions at low concentration (0.005 mg/mL) were also performed, as shown in Fig. 4(a) (CHCl₃-based solutions) and (b) (CHCl₃ + C_5H_{10} -based solutions). The spectra are reproducible and were taken 24 hrs after solution preparation. Once again, no signs of aggregation between 0 and 24 hrs, for the CHCl₃ and CHCl₃ + C_5H_{10} solutions. After 24 hrs, however, aggregate formation in CHCl₃ + C_5H_{10} similar to those observed for high concentration solutions also occurs. This indicates that aggregate formation over time is majorly driven by C_5H_{10} and not by the concentration of the solution. As

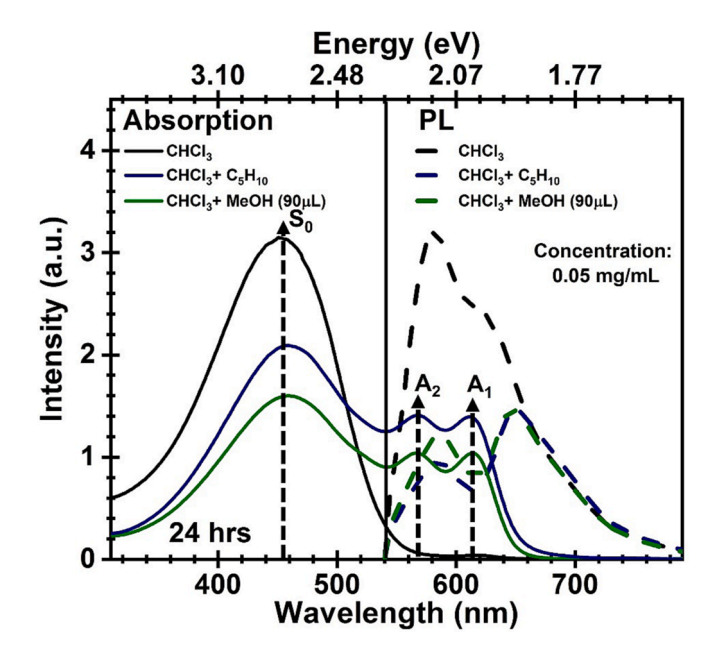


Fig. 3. Absorption (Abs) (solid curves) and Photoluminescence (PL) (dashed curves) spectra for P3HT/CHCl $_3$ (black curves), P3HT/CHCl $_3$ + C $_5$ H $_{10}$ (navy curves), and P3HT/CHCl $_3$ + MeOH (90 μ L) (olive curves) solutions at 24 hrs. The center peaks for the vibronic progressions in (b) are A $_1$ = 613 nm and A $_2$ = 568 nm. The center peak for the isolated chains (i.e. amorphous phase) is S $_0$ = 455 nm.

discussed below, the concentration will not influence the type of aggregate formed (H-aggregate) but will change their exciton bandwidths and $J_{\rm inter}$, which might have a direct influence in the performance of a device. In addition, the study at low concentration is advantageous because it eliminates the previously mentioned IF and SA effects [63] and evaluate, therefore, the true emission profile of the emerging aggregates. Also, even at lower concentrations, solutions with MeOH aggregate instantaneously and remains unchanged over 24 hrs. The amount of MeOH is also varied, and now aliquots of 90 μL and 270 μL are added to both P3HT/CHCl $_3$ + MeOH (Fig. 4(a)) and P3HT/CHCl $_3$ + C_5H_{10} + MeOH (Fig. 4(b)) solutions.

Fig. 4(a) shows the low concentration PL and Abs spectra from solutions of P3HT/CHCl₃, P3HT/CHCl₃ + MeOH (90 µL) and P3HT/CHCl₃ + MeOH (270 μ L), in which 270 μ L of MeOH is added to CHCl₃. When compared to the results in Fig. 3 (see olive solid curve), it is seen that the same H-aggregates structuration are produced and the difference between P3HT/CHCl $_3$ + MeOH (90 μL) and P3HT/CHCl $_3$ + MeOH (270 μ L) seems to be the amount of aggregates formed. Indeed the A_1/A_2 ratio, see Table 1, is 0.95 for both P3HT/CHCl₃ + MeOH (90 µL) and P3HT/CHCl₃ + MeOH (270 μ L). When compared with the A_1/A_2 ratio of 0.99 found for the high concentration P3HT/CHCl₃ + MeOH (90 µL) solutions (see Fig. 3), the A_1/A_2 ratio of 0.95 confirms that variations in concentration affect the J_{inter} magnitudes. The presence of an isosbestic point around 500 nm suggests that the decrease in the number of amorphous chains is equal to the number of aggregates formed. In other words, at low concentrations, different aliquots of MeOH only change the amounts of aggregates formed but not their properties. No effects associated with solvatochromism are observed neither with relation to the high concentration P3HT/CHCl₃ + MeOH (90 μL) case (Fig. 3) nor after changing the MeOH aliquots. This indicates that, although worsening the CHCl3 quality as a good solvent, the addition of MeOH is not substantially changing the CHCl3 polarity. It is noteworthy that the PL spectrum no longer shows evidences for IF and SA effects and the PL from isolated chains (black dashed curve) and from the aggregates (navy and olive dashed curves) are rather similar, confirming that the H-aggregates formed are in the weakly coupled regime, where their emission are dominated by chain-backbones in the H-aggregate structure [30,31,39-41,44-46].

Fig. 4(b) shows the low concentration PL and Abs spectra from $P3HT/CHCl_3 + C_5H_{10}$ at 0hrs, $P3HT/CHCl_3 + C_5H_{10}$ at 24 hrs, $P3HT/CHCl_3 + C_5H_{10}$ $\text{CHCl}_3 + \text{C}_5\text{H}_{10} + \text{MeOH}$ (90 $\mu\text{L}) \text{ and } \text{P3HT/CHCl}_3 + \text{C}_5\text{H}_{10} + \text{MeOH}$ (270 µL) solutions. This time the MeOH aliquots were added to the stabilized CHCl₃ (i.e. CHCl₃ + C_5H_{10}). In one hand, the PL spectra show no signs of IF and SA phenomena and follow the profile observed for the isolated chains, in which the aggregates' emission are dominated by the chain-backbones in the H-aggregate structure (weakly coupled regime). The Abs spectra, on the other hand, show that the vibronic progressions A₁ and A₂ are blueshifted in energy (decrease in wavelength) for the low concentration P3HT/CHCl₃ + C₅H₁₀ at 24hrs solution (see gray-solid curve in Fig. 4(b)) when compared against its high concentration $P3HT/CHCl_3 + C_5H_{10}$ at 24hrs counterpart (see the navy solid curve in Fig. 3), which in turn possess the same A_1 and A_2 peak positions observed for the high concentration P3HT/CHCl $_3$ + MeOH (90 μ L) case (Fig. 3). By recalling that no solvatochromism is observed for the low concentration P3HT/CHCl $_3$ + MeOH (90 μ L and 270 μ L) cases, and since the amount of C5H10 in the solutions is the same, this nonsolvatochromic shift must be associated with the changes in concentration.

Interestingly, the Abs spectra from both low concentration P3HT/ CHCl $_3$ + C_5H_{10} + MeOH (90 μ L) and P3HT/CHCl $_3$ + C_5H_{10} + MeOH (270 μ L) (navy and olive solid curves in Fig. 4(b)) show that the blueshift observed for the vibronic progressions A_1 and A_2 decrease in comparison with the peak positions for the low concentration P3HT/CHCl $_3$ + C_5H_{10} at 24hrs solution (grey solid curve in Fig. 4(b)). This is clear evidence of solvatochromism, in which, contrarily to what is observed for the CHCl $_3$ + MeOH cases, the polarity of the CHCl $_3$ + C_5H_{10} solvent is

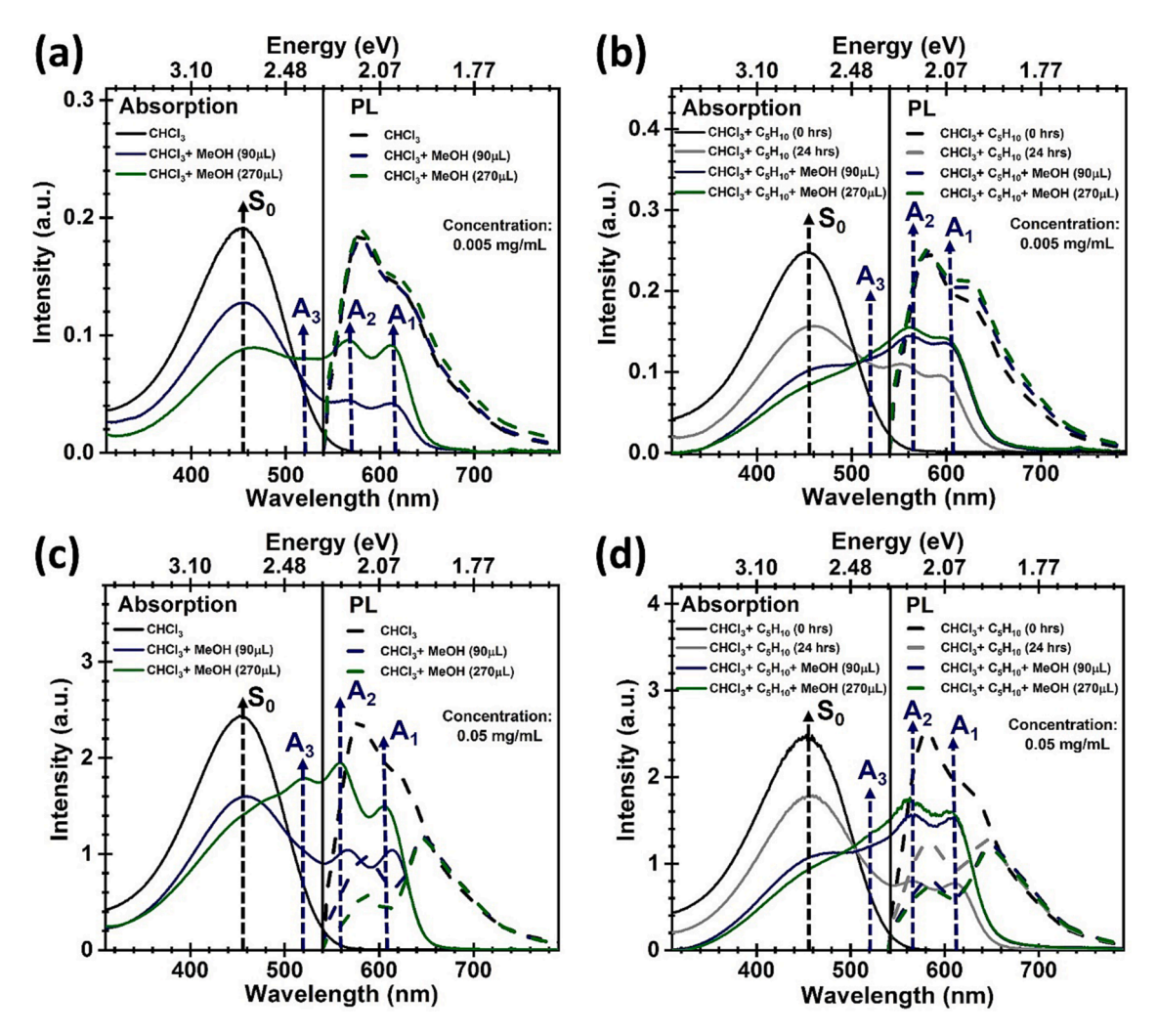


Fig. 4. Absorption (Abs) (solid curves) and Photoluminescence (PL) (dashed curves) spectra for P3HT/CHCl₃ (black curves), P3HT/CHCl₃ + MeOH (90 μL) (navy curves), and P3HT/CHCl₃ + MeOH (270 μL) (olive curves) solutions at 24 hrs: (a) concentration 0.005 mg/mL, where the vibronic progressions are located at $A_1 = 613$ nm, $A_2 = 568$ nm, and $A_3 = 521$ nm for both navy and olive curves (A_3 is not observed for the navy curve), and (c) concentration 0.05 mg/mL, where the vibronic progressions are located at $A_1 = 606$ nm, $A_2 = 559$ nm, and $A_3 = 521$ nm for the olive curve, and $A_1 = 613$ nm and $A_2 = 568$ nm for the navy curve (A_3 is not observed for the navy curve). Absorption (Abs) (solid curves) and Photoluminescence (PL) (dashed curves) spectra for P3HT/CHCl₃ + C_5H_{10} at Ohrs (black curves), P3HT/CHCl₃ + C_5H_{10} (gray curves), P3HT/CHCl₃ + C_5H_{10} + MeOH (90 μL) (navy curves) and P3HT/CHCl₃ + C_5H_{10} + MeOH (270 μL) (olive curves) solutions at 24 hrs: (b) concentration 0.005 mg/mL, where the vibronic progressions are located at $A_1 = 603$ nm, $A_2 = 562$ nm, and $A_3 = 521$ nm for the olive and navy curves, and $A_1 = 595$ nm and $A_2 = 553$ nm for the gray curve (A_3 is not observed for the gray curve), and (d) concentration 0.05 mg/mL, where the vibronic progressions are located at $A_1 = 613$ nm, $A_2 = 568$ nm, and $A_3 = 521$ nm for all the curves (A_3 is not observed for the gray curve). All the figures: the center peak for the isolated chains (i.e. amorphous phase) is $S_0 = 455$ nm.

modified upon the addition of MeOH aliquots. This can be explained by the fact that C₅H₁₀ has several sites for establishing hydrogen bonds with the OH group in MeOH, which is an electronegative group. Usually, the hydrogen bonding capacity along with the dielectric constant are the most important properties in a solvent, being directly associated with the aforementioned solvatochromic effect. In addition, for the P3HT/ $CHCl_3 + C_5H_{10} + MeOH$ (90 µL) and $P3HT/CHCl_3 + C_5H_{10} + MeOH$ (270 μ L) low concentration solutions, the amount of H-aggregates produced are the same, in contrast with the low concentration P3HT/CHCl₃ + MeOH (90 μ L) and P3HT/CHCl $_3$ + MeOH (270 μ L) cases reported in Fig. 4(a), in which the increase of MeOH aliquot leads to the increase in the amount of aggregates. This is further evidence that the presence of C₅H₁₀ do influence the capacity for aggregate formation. The Abs spectra in Fig. 4(b) is less structured than the spectra shown in Fig. 4(a), indicating less planar aggregates [30,31,60-62] with a A₁/A₂ ratio of 0.93 (see Table 1), which is still in agreement with the weakly coupled aggregate regime. There is no longer a common isosbestic point but the crossing point in the PL and Abs from the different solutions are very

close to each other suggesting that, although not one to one, most of amorphous chains are transitioning to the ordered aggregated phase. In other words, C_5H_{10} seems to harden the formation of more planar aggregates.

As seen in Fig. 4(c) (CHCl₃-based solutions) and (d) (CHCl₃ + C₅H₁₀-based solutions), the high concentration regime (0.05 mg/mL), shows the expected concentration-related enhancements in the overall Abs and PL intensities but such enhancements come with other interesting scenarios. In such regime, there is no spectral energy shifts observed for solutions prepared with CHCl₃ + C₅H₁₀ even after MeOH addition, see Fig. 4(d). In other words, it seems that the increase in concentration renders the solvatochromic effect in Fig. 4(b) negligible. Once again, for the P3HT/CHCl₃ + C₅H₁₀ + MeOH (90 μ L) and P3HT/CHCl₃ + C₅H₁₀ + MeOH (270 μ L) high concentration solutions, the amount of H-aggregates produced are essentially the same, in contrast with the high concentration P3HT/CHCl₃ + MeOH (90 μ L) and P3HT/CHCl₃ + MeOH (270 μ L) cases reported in Fig. 4(c), in which the increase (decrease) of MeOH aliquot is associated with the increase (decrease) in the amount of

aggregates. The results replicate those from low concentration samples, which is an indication that even at higher concentrations, the presence of C_5H_{10} renders MeOH ineffective to influence the capacity for aggregate formation. It is also noticeable that in such $C_5H_{10}+\mbox{MeOH}$ solutions, MeOH loses effectiveness in controlling $J_{\rm inter}$ (see the similar A_1/A_2 ratios for both low and high concentrations in Table 1). Indeed, as shown in Fig. 4(d), the Abs spectra shows that no significant differences are observed with changing the MeOH aliquots, except for a slight increase in the vibronic progression A_2 intensity, and for the rise of a weak vibronic progression A_3 in the solution where 270 μL of MeOH is added. The A_1/A_2 ratio is 0.91, while the A_3/A_2 ratio is 0.80 (see Table 1), which indicate that in this case the J_{inter} is essentially unchanged. Similarly to the low concentration case (Fig. 4(b)), there is no common isosbestic point but the crossing point in the Abs from the different

solutions are very close to each other. The conclusion is the same as before: although not one to one, most of amorphous chains are transitioning to the ordered aggregated phase.

An energy blueshift of about 0.14 eV is observed in the Abs spectra with increasing the amount of MeOH from 90 to 270 μL in solutions prepared with CHCl3 (see Fig. 4(c)). Since no solvatochromism is observed at low concentrations (see Fig. 4(a)), this blueshift effect together with the enhanced structuration of the vibronic progressions suggest that the combination of a higher concentration with a higher amount of MeOH is inducing a tighter packing and enhanced H-aggregate behavior, which is consistent with modifications in the $J_{\rm inter}$ magnitude. Such effect has been observed in Lutein H-aggregates [64,65], and it is not strongly observed in $C_5H_{10}+MeOH$ solutions. As expected, both the IF and SA effects are once again observed in the PL

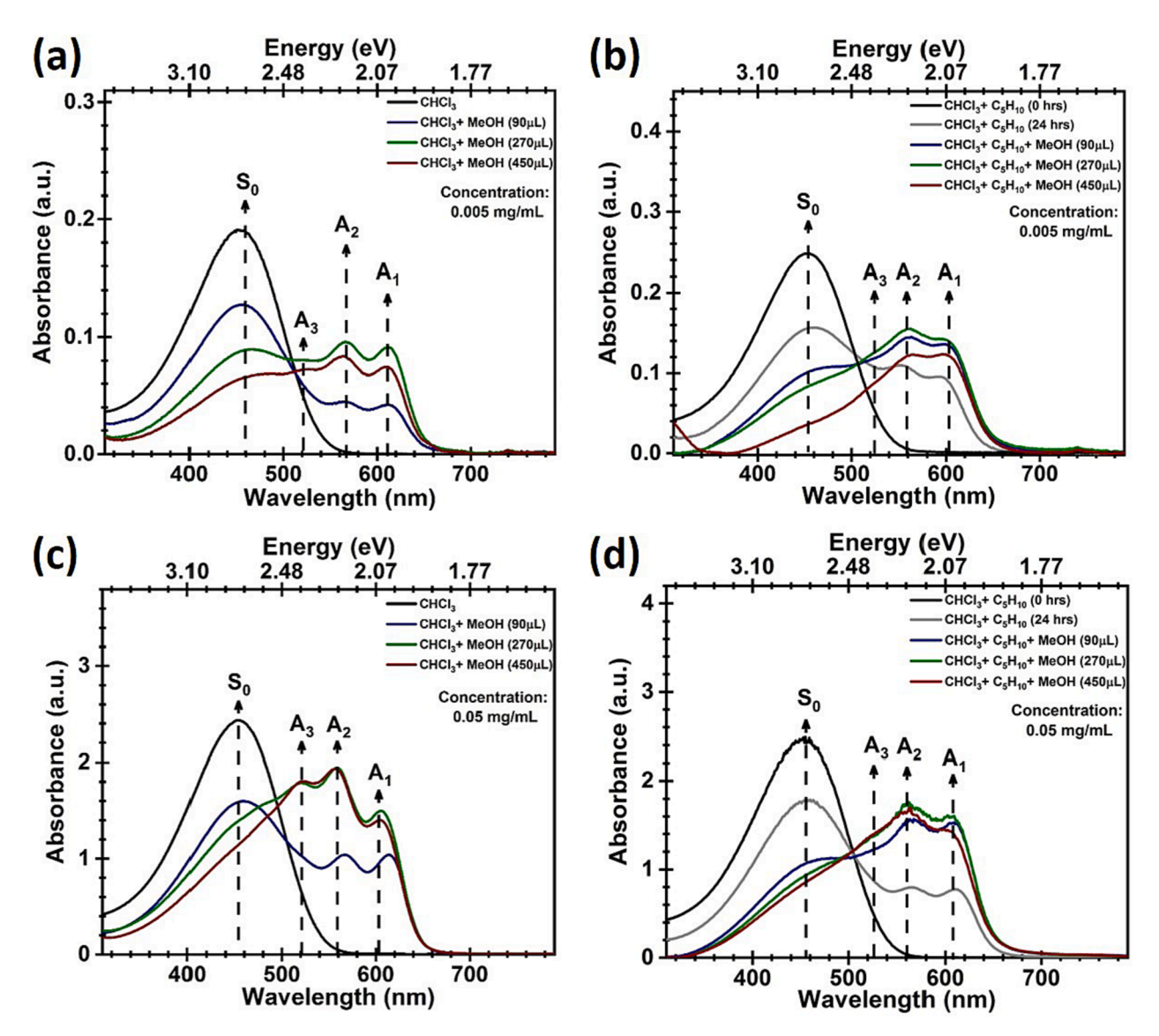


Fig. 5. Absorption (Abs) (solid curves) spectra for P3HT/CHCl₃ (black curves), P3HT/CHCl₃ + MeOH (90 μL) (navy curves), P3HT/CHCl₃ + MeOH (270 μL) (olive curves), and P3HT/CHCl₃ + MeOH (450 μL) (wine curves) solutions at 24 hrs: (a) concentration 0.005 mg/mL, where the vibronic progressions are located at $A_1 = 613$ nm, $A_2 = 568$ nm, and $A_3 = 521$ nm for all the curves (A_3 is not observed for the navy curve), and (c) concentration 0.05 mg/mL, where the vibronic progressions are located at $A_1 = 606$ nm, $A_2 = 559$ nm, and $A_3 = 521$ nm for the olive and wine curves, and $A_1 = 613$ nm and $A_2 = 568$ nm for the navy curve (A_3 is not observed for the navy curve). Absorption (Abs) (solid curves) spectra for P3HT/CHCl₃ + C_5H_{10} at 0hrs (black curves), P3HT/CHCl₃ + C_5H_{10} (gray curves), P3HT/CHCl₃ + C_5H_{10} + MeOH (90 μL) (navy curves), P3HT/CHCl₃ + C_5H_{10} + MeOH (270 μL) (olive curves), and P3HT/CHCl₃ + C_5H_{10} + MeOH (450 μL) (wine curves) solutions at 24 hrs: (b) concentration 0.005 mg/mL, where the vibronic progressions are located at $A_1 = 603$ nm, $A_2 = 562$ nm, and $A_3 = 521$ nm for the navy, olive and wine curves, and $A_1 = 595$ nm and $A_2 = 553$ nm for the gray curve (A_3 is not observed for the gray curve), and (d) concentration 0.05 mg/mL, where the vibronic progressions are located at $A_1 = 613$ nm, $A_2 = 568$ nm, and $A_3 = 521$ nm for all the curves (A_3 is not observed for the gray curve). All the figures: the center peak for the isolated chains (i.e. amorphous phase) is $A_1 = 613$ nm.

but this time, the Abs spectra show that the addition of MeOH is changing the amount of aggregates produced as well as their vibronic progressions' intensities (i.e. J_{inter} is dependent on the MeOH aliquots in the absence of C₅H₁₀). In the case of P3HT/CHCl₃ + MeOH solutions (Fig. 4(c)), it seems that the H-aggregates are not only more structured but also more efficiently formed with increasing the amount of MeOH from 90 to 270 μ L. In addition, the Abs profile from the P3HT/CHCl₃ + MeOH (270 μL) solution shows a third vibronic progression A₃, and now the A_1/A_2 ratio is 0.77, while the A_3/A_2 ratio is 0.92 (see Table 1), which endorses the H-aggregate character of the ordered phase and that modifications in the J_{inter} magnitude are taking place indeed [30,31,39-41,44-46,60-62]. Although there is a clear isosbestic point for the P3HT/CHCl $_3$ + MeOH (90 μ L) solution, in the case of the P3HT/ CHCl₃ + MeOH (270 µL) the shift observed in the Abs crossing point suggest that instead of an equal number of amorphous chains being converted into aggregates in the ordered phase, it might be happening a joint effect of aggregate formation with different planarization as well as distinct planarization of isolated chain in the amorphous phase, which are usually coiled or irregular when fully dissolved in a good solvent such as CHCl₃ [30,31,62]. This type of effect has been suggested in a study by Scharsich and collaborators [31], and it seems to be reduced by the presence of C₅H₁₀ in CHCl₃.

3.2. P3HT as a probe to understand C_5H_{10} and MeOH as agents to control J_{inter} and exciton bandwidths (W)

Fig. 5(a)–(d) focus on a complementary but deeper analysis of representative Abs spectra, at both the low and high concentration regimes, discussed throughout the manuscript. This time, three distinct MeOH aliquots are added to pure (CHCl₃) and stabilized (CHCl₃ + C_5H_{10}) chloroform: 90, 270 and 450 μ L. In all the figures, S_0 stands for the absorption observed for isolated chains (i.e. amorphous phase), and A_i for i=1,2,3 stand for the vibronic progressions. In the weakly coupling regime the ratio A_1/A_2 of vibronic progressions in H-aggregates is approximated by [30,31,39-41,44-46,60-62]:

$$\frac{A_1}{A_2} \approx \left(\frac{1 - 0.24 \left(\frac{W}{E_p}\right)}{1 + 0.073 \left(\frac{W}{E_p}\right)}\right)^2,\tag{1}$$

where W is the exciton bandwidth and E_p is the energy of the main intramolecular vibration coupled to the electronic transition (i.e. the C=C symmetric stretch at 0.18 eV in the case of P3HT) [30,31,39–41,44–46,60–62]. Using Equation (1), the experimental values for A_1/A_2 , and $E_p=0.18$ eV, the exciton bandwidth W can be obtained. The exciton bandwidth is 4 times the J_{inter} magnitude (W = $4|J_{inter}|$), and therefore, J_{inter} can be obtained as well. The weak excitonic coupling regime (i.e. the weakly coupling or polymer regime) occurs whenever W < 0.26 eV [39–41,44–46]. In addition, W is associated with the conjugation length and intrachain order: an increase in conjugation and order leads to a decrease in W. Solving Equation (1) for W results in:

$$W = 4|J_{inter}| \approx E_p \left(\frac{1 - \left(\frac{A_1}{A_2}\right)^{1/2}}{0.24 + 0.073 \left(\frac{A_1}{A_2}\right)^{1/2}} \right)$$
 (2)

Next, a discussion using Equations (1) and (2) is addressed for the several solutions considered above.

Fig. 5(a) shows representative Abs spectra for solutions (concentration 0.005 mg/mL) of P3HT/CHCl₃ (black solid curve), P3HT/CHCl₃ + MeOH (90 μ L) (navy solid curve), P3HT/CHCl₃ + MeOH (270 μ L) (olive solid curve), and P3HT/CHCl₃ + MeOH (450 μ L) (wine solid curve). At this concentration, the A₁/A₂ ratios are 0.95, 0.95, and 0.89 for the solutions with 90, 270, and 450 μ L of MeOH added, respectively (see

Table 1). The vibronic progression A_3 starts to show up for the solutions where 270 and 450 μL are added, and both A_3/A_2 ratios are the same: 0.85. As summarized in Table 1, W = 13 meV and $J_{inter}=3$ meV for the solutions where 90 and 270 μL are added, while W = 32 meV and $J_{inter}=8$ meV for the solutions where 450 μL is added. The increase in the values of W and J_{inter} suggest that the conjugation lengths are decreasing (i.e. lowering the crystalline quality of the aggregate) [30,31,60–62]. As mentioned previously, the isosbestic point observed for the solutions where 90 and 270 μL of MeOH are added suggests a one to one conversion of isolated chains into H-aggregates. This is not the case for the P3HT/CHCl $_3$ + MeOH (450 μL) solution, indicating that the extra amount of MeOH added (67 % more with relation to the 270 μL aliquot) is likely affecting the conformation/planarization of the amorphous chains and aggregates.

In the high concentration regime (0.05 mg/mL), shown in Fig. 5(c), the difference between the P3HT/CHCl₃ + MeOH (270 µL) (olive solid curve) and P3HT/CHCl₃ + MeOH (450 µL) (wine solid curve) are rather small. Therefore, the main conclusions addressed in Section 3.1 hold here. At this concentration, the A_1/A_2 ratios are 0.99, 0.77, and 0.72 for the solutions with 90, 270, and 450 μL of MeOH added, respectively (see Table 1). The vibronic progression A₃ is strong in the solutions where 270 and 450 µL are added, and once more both A₃/A₂ ratios are the same: 0.92, which is in agreement with an enhancement in the H-aggregates' J_{inter} . As summarized in Table 1, $W(J_{inter}) = 0.5 \text{ meV} (0.14 \text{ meV})$ for P3HT/CHCl₃ + MeOH (90 μ L), W (J_{inter}) = 71 meV (18 meV) for P3HT/CHCl $_3$ + MeOH (270 μL), and W (J_{inter}) = 90 meV (22 meV) for P3HT/CHCl $_3$ + MeOH (450 μ L). The increase of MeOH aliquots combined with the increase in concentration is enhancing the H-type character of the aggregates formed, such a combination seems to offer more room for controlling the aggregates' properties, including conjugation length (crystalline quality) of the species in a solution.

Fig. 5(b) shows representative Abs spectra for solutions (concentration 0.005 mg/mL) of P3HT/CHCl $_3$ + C_5H_{10} at 0 hrs (black solid curve), $P3HT/CHCl_3 + C_5H_{10}$ at 24 hrs (gray solid curve), $P3HT/CHCl_3 + C_5H_{10}$ + MeOH (90 μL) (navy solid curve), P3HT/CHCl₃ + C₅H₁₀ + MeOH (270 μ L) (olive solid curve), and P3HT/CHCl $_3$ + C $_5$ H $_{10}$ + MeOH (450 μ L) (wine solid curve). As summarized in Table 1, the A_1/A_2 ratios are 0.85 (for P3HT/CHCl $_3$ + C $_5$ H $_{10}$), 0.93 (for both P3HT/CHCl $_3$ + C $_5$ H $_{10}$ + MeOH (90 $\mu L)$ and P3HT/CHCl $_3$ + C_5H_{10} + MeOH (270 $\mu L)),$ and 0.99 (P3HT/CHCl $_3$ + C_5H_{10} + MeOH (450 $\mu L)$). Also in Table 1 is: W (J_{inter}) = 44 meV (11 meV) for P3HT/CHCl $_3$ + $C_5H_{10},$ W $(J_{\text{inter}}) = 21\,\text{meV}\,(5\,\text{meV})$ for both P3HT/CHCl $_3$ + C_5H_{10} + MeOH (90 $\mu L)$ and P3HT/CHCl $_3$ + C_5H_{10} + MeOH (270 $\mu L)\text{, and }W\left(J_{inter}\right)=2\,\text{meV}\left(0.57\,\text{meV}\right)$ for P3HT/ $CHCl_3 + C_5H_{10} + MeOH$ (450 µL). The values assumed by the parameters are in agreement with our previous discussions and C5H10 seems to be an important player here. In fact, the effect of MeOH in stabilized CHCl₃ is essentially opposite to the effect observed for pure CHCl₃: with increasing the amount of MeOH, W (Jinter) is decreasing, which suggests that the conjugation length and crystalline quality are increasing for these solutions. The H-aggregates are more weakly interacting, which is further confirmed by the decreasing A₃/A₂ ratios with increasing the MeOH aliquots (see Table 1).

In the high concentration regime (0.05 mg/mL), the A_1/A_2 ratios are 0.96 for P3HT/CHCl $_3+C_5H_{10}$ and P3HT/CHCl $_3+C_5H_{10}+$ MeOH (90 $\mu L)$, 0.91 for P3HT/CHCl $_3+C_5H_{10}+$ MeOH (270 $\mu L)$), and 0.85 (P3HT/CHCl $_3+C_5H_{10}+$ MeOH (450 $\mu L)$). In addition (see Table 1): W ($J_{inter})=10$ meV (2 meV) for both P3HT/CHCl $_3+C_5H_{10}$ and P3HT/CHCl $_3+C_5H_{10}+$ MeOH (90 $\mu L)$, W ($J_{inter})=26$ meV (7 meV) for P3HT/CHCl $_3+C_5H_{10}+$ MeOH (270 $\mu L)$, and W ($J_{inter})=45$ meV (11 meV) for P3HT/CHCl $_3+C_5H_{10}+$ MeOH (450 $\mu L)$. This time around, the increase of MeOH aliquots combined with the increase in concentration is once again enhancing the H-type character of the aggregates formed (the A_3/A_2 ratios endorse this conclusion, see Table 1). The gradual increase in W suggests that the conjugation length and the aggregates' crystalline quality are decreasing for these solutions. The results here are similar to the high concentration solutions of pure CHCl $_3$ but much less

pronounced (i.e. $J_{\rm inter}$ and W about 50 % smaller), which is an additional confirmation that C_5H_{10} is in fact rendering MeOH less effective. Differently from the low concentration case, the Abs crossing point between the P3HT/CHCl $_3$ + C_5H_{10} and P3HT/CHCl $_3$ + C_5H_{10} + MeOH (450 μL) is much closer to the crossing points observed for the other solutions. This suggests that an isosbestic point is being recovered and so it is the one to one conversion from amorphous chains into ordered aggregates.

4. Conclusions

In this manuscript, H-aggregate formation in CHCl $_3$ -based P3HT solutions is used as probes to investigate the role of C_5H_{10} and its association with MeOH in determining the solvent's quality. It is shown that pure and C_5H_{10} -stabilized CHCl $_3$ lead to distinct aggregate properties in both their pristine and MeOH-modified conditions. It is seen that C_5H_{10} renders MeOH ineffective to alter the CHCl $_3$ polarity, to control the amount of aggregate formation as well as to control the planarity and crystallinity of the aggregates formed. In addition, it is seen that C_5H_{10} , which is often used as a CHCl $_3$ stabilizer, limits the lifespan of CHCl $_3$ as a good solvent, leading to aggregate formation in 24 h after solution preparation. Moreover, it is shown that the combination of both C_5H_{10} and several aliquots of MeOH opens up additional routes for controlling both the exciton bandwidth and J_{inter} magnitude when compared with routes where only aliquots of MeOH are changed.

CRediT authorship contribution statement

Huan Nguyen: Conceptualization, Data curation, Formal analysis, Investigation, Validation, Writing – original draft, Software. Ruan L.S. Lima: Conceptualization, Data curation, Formal analysis, Investigation, Validation, Writing – original draft, Software. Newton M. Barbosa Neto: Conceptualization, Data curation, Formal analysis, Funding acquisition, Investigation, Supervision, Validation, Visualization, Writing – original draft, Writing – review & editing. Paulo T. Araujo: Conceptualization, Data curation, Formal analysis, Funding acquisition, Investigation, Methodology, Project administration, Resources, Supervision, Validation, Visualization, Writing – original draft, Writing – review & editing.

Declaration of competing interest

The authors declare that they have no known competing financial interests or personal relationships that could have appeared to influence the work reported in this paper.

Data availability

Data will be made available on request.

Acknowledgements

The authors are indebted to Brazilian agencies: CNPq under Grants No. [306147/2020-3], FAPESPA and CAPES under Grant No. [Finance Code 001; AUXPE 88881.159129/2017-01]. NMBN acknowledges the support from the Brazilian National Council for Scientific and Technological Development (CNPq) (process number: 465572/2014-6), the São Paulo Research Foundation. PTA is grateful to the National Science Foundation (NSF) under Grant No. [1848418] for the financial support. NMBN is especially grateful to Fulbright Foundation for the Visiting Professor Scholarship Award.

References

[1] N.V. Handa, et al., Exploring the synthesis and impact of end-functional poly (3-hexylthiophene), J. Polym. Sci. A: Polym. Chem. 53 (7) (2015) 831–841.

- [2] N.J. Hestand, et al., Exciton mobility control through sub— Å packing modifications in molecular crystals, Phys. Rev. B 91 (19) (2015) 195315.
- [3] S. Kilina, D. Kilin, S. Tretiak, Light-driven and phonon-assisted dynamics in organic and semiconductor nanostructures, Chem. Rev. 115 (12) (2015) 5929–5978.
- [4] Y. Liang, et al., 50th anniversary perspective: polymeric biomaterials: diverse functions enabled by advances in macromolecular chemistry, Macromolecules 50 (2) (2017) 483–502.
- [5] P. Musto, Grand challenges in polymer chemistry: energy, environment, health, Front. Chem. 1 (2013) 31.
- [6] O. Ostroverkhova, Organic optoelectronic materials: mechanisms and applications, Chem. Rev. 116 (22) (2016) 13279–13412.
- [7] R. Stepto, et al., Mission and challenges of polymer science and technology, Pure Appl. Chem. 75 (10) (2003) 1359–1369.
- [8] D. Wang, et al., From single chains to aggregates, how conjugated polymers behave in dilute solutions, Macromolecules 46 (15) (2013) 6217–6224.
- [9] B. Valeur, M.N. Berberan-Santos, Molecular Fluorescence: Principles and Applications, John Wiley & Sons, 2012.
- [10] P. Bi, et al., Achieving 31% efficiency in organic photovoltaic cells under indoor light using a low energetic disorder polymer donor, J. Mater. Chem. A 11 (2023) 983.
- [11] S. Smeets, et al., Structurally pure and reproducible polymer materials for highperformance organic solar cells, Chem. Mater. 35 (2023) 8158–8169.
- [12] K. Yamanaka, et al., Interplay between π-conjugated polymer donors and acceptors determines crystalline order of their blends and photovoltaic performance, Adv. Energy Mater. 13 (2023) 2203443.
- [13] B. Zhang, et al., Superior high-temperature energy density in molecularsemiconductor/polymer all-organic composites, Adv. Funct. Mater. 33 (2023) 2210050.
- [14] X. Yuan, et al., Benzo[1,2-b:4,5-b']difuran-based polymer for organic solar cells with 17.5% efficiency via halogenation-mediated aggregation control, Adv. Energy Mater. 13 (2023) 2204394.
- [15] J. Wang, et al., A new polymer donor enables binary all-polymer organic photovoltaic cells with 18% efficiency and excellent mechanical robustness, Adv. Mater. 34 (2022) 2205009.
- [16] J. Wang et al., Low-cost fully non-fused ring acceptor enables efficient organic photovoltaic modules for multi-scene applications. Angew. Chem. Int. Ed. (2023) e202314362 (1 of 12), doi: 10.1002/anie.202314362.
- [17] K. Xian, et al., Simultaneous optimization of efficiency, stretchability, and stability in all polymer solar cells via aggregation control, Chin. J. Chem. 41 (2023) 159–166.
- [18] Z.-F. Yao, J.-Y. Wang, J. Pei, Controlling morphology and microstructure of conjugated polymers via solution-state aggregation, Prog. Polym. Sci. 136 (2023) 101626.
- [19] B. Zhang, F. Yang, Y. Li, Recent progress in large-area organic solar cells, Small Sci. 3 (2023) 2300004.
- [20] C. Liu, et al., Recent progress in π -conjugated polymers for organic photovoltaics: solar cells and photodetectors, Prog. Polym. Sci. 143 (2023) 101711.
- [21] T. Faraco, et al., Review of bacterial nanocellulose as suitable substrate for conformable and flexible organic light-emitting diodes, Polymers 15 (2023) 479.
- [22] P.M. Reichstein, et al., Influence of composition of amphiphilic double-crystalline P3HT-b-PEG block copolymers on structure formation in aqueous solution, Macromolecules 49 (2016) 5484–5493.
- [23] S.L. Fronk, et al., End-group-mediated aggregation of poly(3-hexylthiophene), Macromolecules 48 (2015) 6224–6232.
- [24] P. Beer, et al., Disorder in P3HT nanoparticles probed by optical spectroscopy on P3HT-b-PEG micelles, Chem. A Eur. J. 125 (2021) 10165–10173.
- [25] E.H. Kwon, et al., Effect of alcohol polarity on the aggregation and film-forming behaviors of poly(3-hexylthiophene), ACS Appl. Polym. Mater. 2 (2020) 2980–2986.
- [26] S.-M. Jin, et al., Precrystalline P3HT nanowires: growth controllable solution processing and effective molecular packing transfer to thin film, CrstEngComm 24 (2022) 1248.
- [27] M. Baghgar, et al., Probing inter-and intrachain exciton coupling in isolated poly (3-hexylthiophene) nanofibers: effect of solvation and regioregularity, J. Phys. Chem. Lett. 3 (12) (2012) 1674–1679.
- [28] P. Ehrenreich, et al., H-aggregate analysis of P3HT thin films-capability and limitation of photoluminescence and UV/Vis spectroscopy, Sci. Rep. 6 (2016) 32434.
- [29] E.T. Niles, et al., J-aggregate behavior in poly-3-hexylthiophene nanofibers, J. Phys. Chem. Lett. 3 (2) (2012) 259–263.
- [30] F. Panzer, et al., Spectroscopic signature of two distinct H-aggregate species in poly (3-hexylthiophene), Macromolecules 48 (5) (2015) 1543–1553.
- [31] C. Scharsich, et al., Control of aggregate formation in poly (3-hexylthiophene) by solvent, molecular weight, and synthetic method, J. Polym. Sci. B 50 (6) (2012) 442–453.
- [32] M. Baghgar, et al., Effect of polymer chain folding on the transition from H-to J-aggregate behavior in P3HT nanofibers, J. Phys. Chem. C 118 (4) (2014) 2229–2235.
- [33] J.A. Labastide, et al., Time-and polarization-resolved photoluminescence decay from isolated polythiophene (P3HT) nanofibers, J. Phys. Chem. C 116 (44) (2012) 23803–23811.
- [34] F.C. Spano, Modeling disorder in polymer aggregates: the optical spectroscopy of regioregular poly (3-hexylthiophene) thin films, J. Chem. Phys. 122 (23) (2005) 234701.

- [35] F.C. Spano, et al., Determining exciton coherence from the photoluminescence spectral line shape in poly (3-hexylthiophene) thin films, J. Chem. Phys. 130 (7) (2009) 074904.
- [36] E.S. Manas, F.C. Spano, Absorption and spontaneous emission in aggregates of conjugated polymers, J. Chem. Phys. 109 (18) (1998) 8087–8101.
- [37] T. Nakano, Synthesis, structure and function of π -stacked polymers, Polym. J. 42 (2) (2010) 103–123.
- [38] F.C. Spano, Excitons in conjugated oligomer aggregates, films, and crystals, Annu. Rev. Phys. Chem. 57 (2006) 217–243.
- [39] F.C. Spano, The spectral signatures of Frenkel polarons in H-and J-aggregates, Acc. Chem. Res. 43 (3) (2009) 429–439.
- [40] F.C. Spano, C. Silva, H-and J-aggregate behavior in polymeric semiconductors, Annu. Rev. Phys. Chem. 65 (2014) 477–500.
- [41] F.C. Spano, H. Yamagata, Vibronic coupling in J-aggregates and beyond: a direct means of determining the exciton coherence length from the photoluminescence spectrum, J. Phys. Chem. B 115 (18) (2010) 5133–5143.
- [42] R. Traiphol, et al., Chain organization and photophysics of conjugated polymer in poor solvents: aggregates, agglomerates and collapsed coils, Polymer 48 (3) (2007) 813-826
- [43] F. Würthner, T.E. Kaiser, C.R. Saha-Möller, J-Aggregates: from serendipitous discovery to supramolecular engineering of functional dye materials, Angew. Chem. Int. Ed. 50 (15) (2011) 3376–3410.
- [44] H. Yamagata, et al., HJ-aggregate behavior of crystalline 7, 8, 15, 16-tetraazater-rylene: introducing a new design paradigm for organic materials, J. Phys. Chem. C 118 (49) (2014) 28842–28854.
- [45] H. Yamagata, F.C. Spano, Interplay between intrachain and interchain interactions in semiconducting polymer assemblies: the HJ-aggregate model, J. Chem. Phys. 136 (18) (2012) 184901.
- [46] N.J. Hestand, F.C. Spano, Molecular aggregate photophysics beyond the Kasha model: novel design principles for organic materials, Acc. Chem. Res. 50 (2) (2017) 341, 350.
- [47] G.A. Sherwood, et al., Aggregation effects on the emission spectra and dynamics of model oligomers of MEH-PPV, J. Phys. Chem. C 113 (2009) 18851.
- [48] S.H. Chen, et al., Aging of poly(2-methoxy-5-(2¢-ethylhexyloxy)-1,4-phenylenevinylene)/toluene solutions and subsequent effects on luminescence behavior of cast films, Langmuir 20 (2004) 8909.
- [49] A. Köhler, S.T. Hoffmann, H. Bässler, An order—disorder transition in the conjugated polymer MEH-PPV, J. Am. Chem. Soc. 134 (2021) 11594.
- [50] T.-Q. Nguyen, et al., Controlling interchain interactions in conjugated polymers: the effects of chain morphology on exciton-exciton annihilation and aggregation in MEH-PPV films, J. Phys. Chem. B 104 (2000) 237.

- [51] K. Koynov, et al., Molecular weight dependence of chain orientation and optical constants of thin films of the conjugated polymer MEH-PPV, Macromolecules 39 (2006) 8692.
- [52] S. Habuchi, S. Onda, M. Vacha, Molecular weight dependence of emission intensity and emitting sites distribution within single conjugated polymer molecules, PCCP 13 (2011) 1743.
- [53] Z. Xu, H. Tsai, H.-L. Wang, M. Cotlet, Solvent polarity effect on chain conformation, film morphology, and optical properties of a water-soluble conjugated, Polymer, J. Phys. Chem. B 114 (2010) 11746.
- [54] D.M. Bielinskia, et al., Modification of polymer materials by ion bombardment: case studies, AIP Conf. Proc. 1099 (2009) 357.
- [55] K. Haraguchi, Synthesis and properties of soft nanocomposite materials with novel organic/inorganic network structures, Polym. J. 43 (2011) 223–241.
- [56] T. Miyata, Preparation of smart soft materials using molecular complexes, Polym. J. 42 (2010) 277–289.
- [57] M. Knaapila, et al., Measuring structural inhomogeneity of conjugated polymer at high pressures up to 30 GPa, Macromolecules 46 (2013) 8284–8288.
- [58] Y.-C. Xu, et al., Conjugated polymers in solution: a physical perspective, J. Phys. Chem. Lett. 14 (2023) 927–939.
- [59] Z.E. Lampert, et al., Controlling morphology and chain aggregation in semiconducting conjugated polymers: the role of solvent on optical gain in MEH-PPV, J. Phys. Chem. B 116 (2012) 12835–12841.
- [60] M. Chang, J. Lee, N. Kleinhenz, B. Fu, E. Reichmanis, Photoinduced anisotropic supramolecular assembly and enhanced charge transport of poly(3hexylthiophene) thin films, Adv. Funct. Mater. 24 (2014) 4457.
- [61] N.M.B. Neto, et al., Photoinduced self-assembled nanostructures and permanent polaron formation in regionegular poly (3-hexylthiophene), Adv. Mater. 30 (2018) 1705052.
- [62] J. Clark, et al., Determining exciton bandwidth and film microstructure in polythiophene films using linear absorption spectroscopy, Appl. Phys. Lett. 94 (2009) 163306.
- [63] S.K. Panigrahi, A.K. Mishra, Inner filter effect in fluorescence spectroscopy: as a problem and as a solution, J. Photochem. Photobiol. C: Photochem. Rev. 41 (2019) 100318
- [64] F. Zsila, et al., Investigation of the selforganization of lutein and lutein diacetate by electronic absorption, circular dichroism spectroscopy, and atomic force microscopy, J. Phys. Chem. B 105 (2001) 9413–9421.
- [65] F.C. Spano, Analysis of the UV/vis and CD spectral line shapes of carotenoid assemblies: spectral signatures of chiral H-aggregates, J. Am. Chem. Soc. 131 (2009) 4267–4278.